

In Vivo Confocal Imaging of Fluorescently Labeled Microbubbles: Implications for Ultrasound Localization Microscopy

Matthew R. Lowerison¹, Chengwu Huang¹, *Member, IEEE*, Yohan Kim, Fabrice Lucien, Shigao Chen², *Senior Member, IEEE*, and Pengfei Song¹, *Senior Member, IEEE*

Abstract—We report the time kinetics of fluorescently labeled microbubbles (MBs) in capillary-level microvasculature as measured via confocal microscopy and compare these results to ultrasound localization microscopy (ULM). The observed 19.4 ± 4.2 MBs per confocal field-of-view ($212 \mu\text{m} \times 212 \mu\text{m}$) are in excellent agreement with the expected count of 19.1 MBs per frame. The estimated time to fully perfuse this capillary network was 193 s, which corroborates the values reported in the literature. We then modeled the capillary network as an empirically determined discrete-time Markov chain with adjustable MB transition probabilities through individual capillaries. The Monte Carlo random walk simulations found perfusion times ranging from 24.5 s for unbiased Markov chains up to 182 s for heterogeneous flow distributions. This pilot study confirms a probability-derived explanation for the long acquisition times required for super-resolution ULM.

Index Terms—Microbubble (MB) tracking, microvasculature, super-resolution, ultrasound microvessel imaging.

I. INTRODUCTION

ULTRASOUND localization microscopy (ULM) is a super-resolution imaging technique that overcomes the conventional diffraction limit of ultrasound imaging by exploiting the unique acoustic properties of contrast microbubbles (MBs) in vasculature [1]–[5]. ULM processing results in an approximately tenfold improvement in vascular imaging resolution [1] while preserving clinically relevant penetration depths and maintaining the safety, low-cost, and lack of ionizing radiation of ultrasound. Thus, ULM offers unprecedented

clinical significance by providing noninvasive, *in vivo* blood flow information potentially down to the capillary scale—which may be critical in informing a broad spectrum of pathological disease states. However, ULM is currently limited by long imaging acquisition times for the full reconstruction of microvascular networks, which represents a substantial barrier to clinical translation of the technique. A prevailing hypothesis is that these long acquisition times are a natural consequence of the rare occurrence of MB passage in capillary vessels [6], [7]. Conversely, previous studies have demonstrated that the MB signal becomes attenuated inside capillaries due to the constraints in volumetric expansion from vessel walls [8]–[11], which may partially explain the difficulty in reconstructing capillary networks with ULM.

A number of different investigators have explored the fundamental tradeoff between ULM microvascular fidelity and imaging acquisition times. Dencks *et al.* [12] investigated the minimum time required to reconstruct microvascular trees via ULM from murine tumor xenografts. They reported 90% microvessel mapping times, based on an exponential saturation fitting, of 50–101 s. Hingot *et al.* [6] compared the relationship between ULM pixel reconstruction size and acquisition time in the murine brain, finding a characteristic time of 76.8 s for ULM reconstructions at $5 \mu\text{m}$. This corresponds to a 90% saturation time of 230.4 s. Christensen-Jeffries *et al.* [7] developed a Poisson statistical model to predict ULM acquisition times for generalized imaging conditions and target vasculature. When applying their model to the experimental conditions reported in Dencks *et al.*'s work, they found estimated perfusion times ranging from 78 to 139 s. The salient conclusion from these studies is that the long acquisition times required for ULM reconstruction of microvasculature is inherently a consequence of vessel physiology, flow rates, and the low probability of MB passage through capillaries. It is worth noting, however, that the standards that are often used in investigations of ULM performance are either ultrasound imaging itself (i.e., comparing long acquisition times with shorter duration subsets) or are histological metrics that provide static physiological quantifications (e.g., microvascular density), which may be difficult to register to a corresponding imaging plane.

The objective of this article is to explore flow kinetics of MBs *in vivo* using high framerate ultrasound and confocal microscopy as MBs traverse through the chorioallantoic

Manuscript received March 13, 2020; accepted April 12, 2020. Date of publication April 15, 2020; date of current version August 27, 2020. This work was supported in part by the National Institutes of Health (NIH) under Grant R00CA214523 and Grant R01DK120559. (*Corresponding author: Pengfei Song.*)

Matthew R. Lowerison and Pengfei Song are with the Beckman Institute, University of Illinois at Urbana–Champaign, Urbana, IL 61801 USA, also with the Department of Electrical and Computer Engineering, University of Illinois at Urbana–Champaign, Urbana, IL 61801 USA, and also with the Department of Radiology, Mayo Clinic College of Medicine and Science, Rochester, MN 55905, USA (e-mail: songp@illinois.edu).

Chengwu Huang and Shigao Chen are with the Department of Radiology, Mayo Clinic College of Medicine and Science, Rochester, MN 55905, USA.

Yohan Kim and Fabrice Lucien are with the Department of Urology, Mayo Clinic College of Medicine and Science, Rochester, MN 55905, USA.

This article has supplementary downloadable material available at <http://ieeexplore.ieee.org>, provided by the authors.

Digital Object Identifier 10.1109/TUFFC.2020.2988159

membrane (CAM) of chicken embryos. The *ex ovo* CAM offers an excellent exploratory model for MB flow kinetics due to the well-organized planar vascular bed developed by the membrane, which is optically transparent and readily accessible. This permits rapid coregistered acoustic–optic studies of MB transit using multiple imaging modalities. Confocal microscopy provides an imaging resolution that is in the submicron range and, thus, serves as a reliable benchmark for the identification of fluorescently labeled MBs. Here, we report that the time kinetics of fluorescently labeled MBs, taken from the superficial vascular bed of the CAM, are in good agreement with a probability-derived explanation for long acquisition times required for ULM imaging. Confocal imaging allowed for the visualization of MBs as they traversed through the CAM vessel bed. It was noted that there was a heterogeneous distribution of MBs through this capillary bed, leading to some capillary segments being rarely traversed by MBs. We then modeled this capillary bed as an empirically determined discrete-time Markov chain network and estimated perfusion times using a Monte Carlo random-walk simulation. The effect of adjusting the node-to-node transition weightings on the network coverage time was also explored. This Monte Carlo simulation permitted the investigation of rare MB passage events on the anticipated 90% saturation time for a physiologically relevant network connection topology. We found that unbalanced transition probabilities, arising from heterogeneous MB flow through the capillary bed, can extend the estimate for full perfusion by at least an order of magnitude.

The rest of this article is structured as follows. In Section II, we introduce the *ex ovo* CAM preparation, the steps involved in super-resolution ULM imaging, and the confocal imaging procedure, along with the Monte Carlo simulation details. In Section III, we show the results of estimates for time to complete perfusion based on ULM imaging, confocal imaging, and Monte Carlo simulations. We then discuss these results in Section IV and provide a conclusion.

II. MATERIALS AND METHODS

A. Ex Ovo CAM Preparation

Avian embryos, such as the CAM model used in this study, are not considered to be “live vertebrate animals” under NIH public health service (PHS) policy. As such, no Institutional Animal Care and Use Committee (IACUC) approval was necessary to conduct the research presented in this article.

Fertilized chicken eggs (white leghorn) were obtained from Hoover’s Hatchery (Rudd, IA, USA) and immediately placed into an incubator upon receipt (Digital Sportsman Cabinet Incubator 1502, GQF). This was counted as the first day of embryonic development (EDD-01). On EDD-04, the eggshells were removed with the aid of a rotary Dremel tool, and the egg contents were transferred into plastic weigh boats prepared with acoustic windows. Embryos were kept in a humidified incubator (Caron model 7003-33) until imaging on EDD-18. A total of three chicken embryos was used in this pilot study.

A vial of “target-ready” Vevo Micromarker (FUJIFILM VisualSonics) was reconstituted with 1-mL phosphate-buffered saline (PBS) and 0.25 μg Biotin-4-fluorescein, yielding a

solution of 2×10^9 fluorescein isothiocyanate (FITC)-labeled MBs/mL. A solution of rhodamine lectin (lens culinaris agglutinin) was prepared in advance of imaging at a 1:10 dilution with PBS. Prior to injection, glass capillary needles were produced by pulling borosilicate glass tubes (1.20 mm \times 0.69 mm \times 10 cm, Sutter Instruments, Novato, CA, USA) with a PC-100 glass puller (Narishige, Setagaya City, Japan) and fit onto Tygon R-3603 laboratory tubing. On EDD-18, the surface vasculature of the CAM was cannulated with the glass capillary needle, and 100 μL of the rhodamine lectin solution was injected to fluorescently label the vascular endothelium [13]. Following this, the embryo was returned to the incubator for 15 min to allow complete recirculation and labeling of the lectin. Immediately prior to imaging, the CAM membrane was injected with a 70- μL bolus of FITC-labeled MBs.

B. Ultrasound Imaging

Ultrasound images were acquired using a Vantage 256 system (Verasonics Inc., Kirkland, WA, USA). A high-frequency linear array transducer (L35-16vX, Verasonics Inc.) was placed on the side of the plastic weigh boat housing the CAM to image through the acoustic window. Center frequency was 20 MHz, selected to reconstruct a capillary-scale super-resolved image [14]. Imaging was performed using a nine-angle plane-wave compounding sequence (1° increment step) with a postcompounding frame rate of 1000 Hz for a total acquisition length of 32 s (32 000 frames). Ultrasound images were stored as in-phase quadrature (IQ) data sets of 1600 frames each for analysis in MATLAB.

Super-resolution MB localization and velocity maps were reconstructed at a 5- μm axial/lateral resolution following the methodology presented in [5]. Briefly, each IQ data set was reshaped into a 2-D Casorati matrix and separated into singular values via singular value decomposition (SVD). A low-order threshold was applied to filter out tissue background [15], where the threshold was determined by the decay rate of the singular value curve [5]—a threshold value of 10 for each 1600 frames data set. A filtered Casorati matrix was generated via inverse SVD and reshaped back into the original cine-loop dimensions. A normalized cross correlation was then performed on each frame of the cine-loop with a Gaussian function, representing the point-spread function of an individual MB, to localize MB centroids. MBs trajectories were then reconstructed using a normalized cross correlation algorithm to track MB movement and velocity [4].

Optical microscopy was performed simultaneously with ULM imaging using a Nikon SMZ18 stereomicroscope (Nikon, Tokyo, Japan) at 4 \times magnification to confirm the reconstruction of vascular features. A diagrammatic example of the optic–acoustic imaging setup is shown in Fig. 1, demonstrating multiscale optical validation coinciding with acoustic imaging. Following acoustic imaging, a region of interest was selected on the CAM membrane, and confocal microscopy was performed to generate capillary-level vascular images and to optically track individual FITC-MBs.

The optical and acoustic data sets were then spatially coregistered to confirm the accurate reconstruction of vasculature via ULM processing, as shown in Fig. 2.

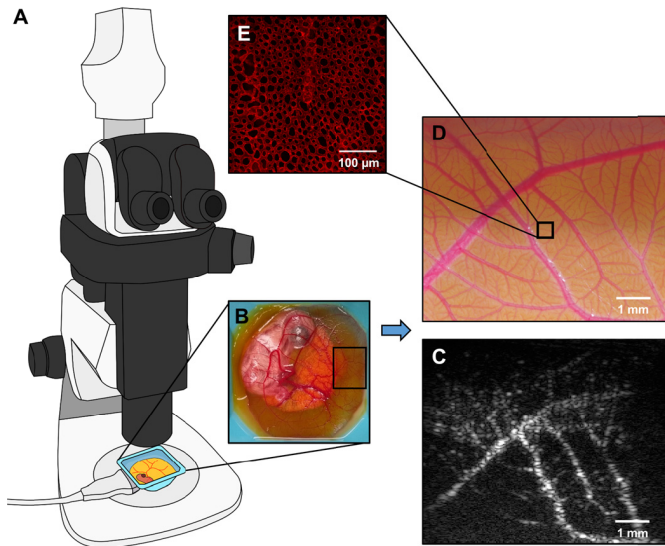


Fig. 1. (a) Diagrammatic example of the coregistered optic-acoustic imaging setup used in this experiment. (b) Chicken embryos were positioned under the stereomicroscope with the ultrasound transducer coupled to the side of the weigh boat. (c) SVD filtered ultrasound image of CAM vasculature, demonstrating MB events. (d) Optical image that served as a reference standard for ULM imaging. (e) Confocal imaging of the CAM vasculature demonstrates a honey comb-like capillary bed.

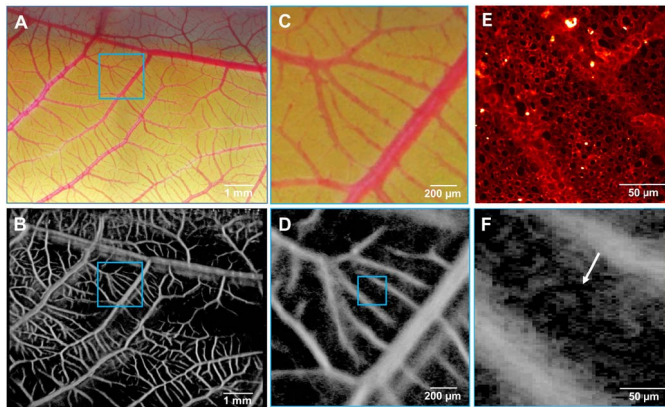


Fig. 2. (a) Optical microscopy image was coregistered with the ultrasound imaging plane and allowed for the identification, localization, and verification of vessels detected by ULM. (b) ULM image of the corresponding CAM vessel network, yielding a similar vascular structure. (c) Higher magnification optical image was acquired to investigate the performance of (d) ULM at the arteriole/venule scale. (e) Confocal imaging of the superficial capillary layer demonstrates a characteristic hexagonal microvascular bed, which was partially recovered with (f) ULM imaging (arrow). Note that the confocal image shown in (e) is for demonstrative purposes only and was not taken from the same CAM membrane shown in the other image panels.

C. Confocal Imaging

Laser-scanning confocal images were acquired using a Nikon AIR+ system following intravascular injection of FITC-labeled Vevo Micromarker MBs and CAM endothelial vessels labeled with rhodamine lectin. Multispectral data were acquired using enhanced green fluorescent protein (eGFP) (emission wavelength 525 nm) and tdTomato (emission wavelength 595 nm) channels. Confocal images had a 212 $\mu\text{m} \times 212 \mu\text{m}$ field of view (FOV), 0.414- μm isotropic resolution, and a framerate of 14.7 Hz. Images were digitized at 16 bits using an integrated digital camera and saved as .nd2 format.

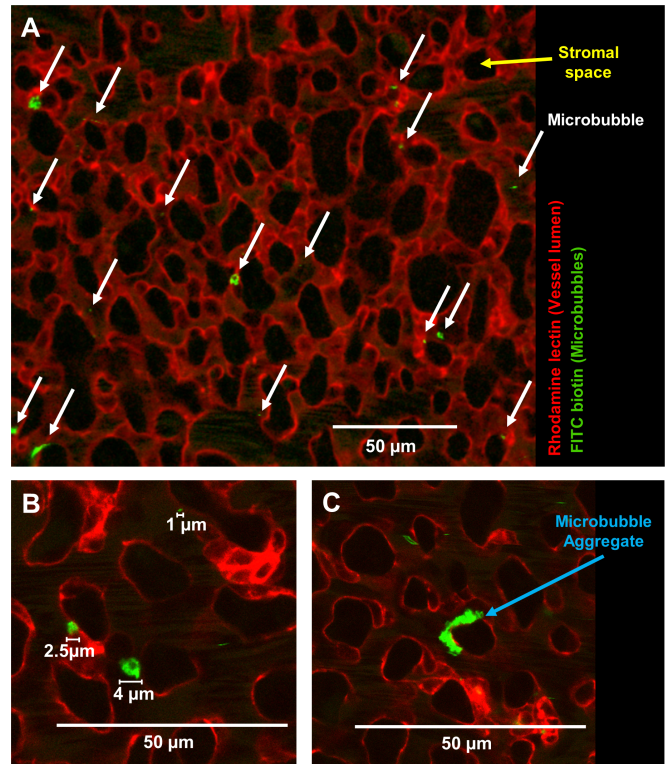


Fig. 3. (a) Confocal imaging of the superficial CAM vascular bed. The vascular lumen is stained with rhodamine lectin (red channel), and MBs were labeled with FITC (green channel). Black spaces are stromal space. (b) Further magnified image of the vessel bed highlights the polydisperse size distribution MBs. (c) Example of a large MB event, indicating potential MB aggregation.

Fig. 3 demonstrates a representative example image of a confocal imaging FOV used in this study.

Image channels were split and then exported as .PNG files for offline analysis in MATLAB. MBs were detected using a 2-D normalized cross correlation on the eGFP channel data with a hypothetical 2-D Gaussian bubble profile [16]. A cross-correlation threshold of 0.5 was used to reject low confidence MB detections, and MB diameters were estimated from the eGFP channel data assuming a circular cross section (see **Fig. 4**). This was validated using an AccuSizer single-particle optical sizing system (Model 780, Particle Sizing Systems, Santa Barbara, CA, USA) on a 10- μL sample of the FITC-MB conjugate. Total MB counts were then generated for each frame by enumerating isolated MB regions (see **Fig. 5**). The blood volume of each confocal field of view was estimated using watershed segmentation with manually selected seed points placed on stromal regions within the FOV. The number of capillary segments within each confocal plane was estimated using Voronoi tessellation (e.g., “voronoi.m” in MATLAB) on centroids of CAM stromal spaces. An example of this processing is demonstrated in **Fig. 6**.

D. Wash-In Function

Next, we estimated the total time it would take to completely perfuse the capillary bed with MBs (i.e., the time taken to reconstruct the entire vascular network under ideal conditions). We first accumulated all of the ULM data sets to

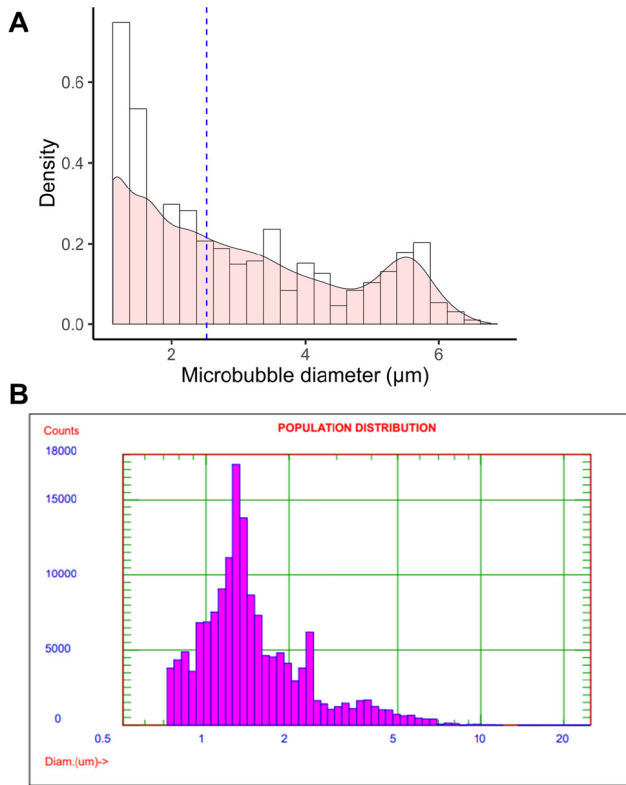


Fig. 4. (a) Empirical density function of MB diameters, with median diameter indicated with a dotted line, which was confirmed with (b) AccuSizer 780 particle sizer.

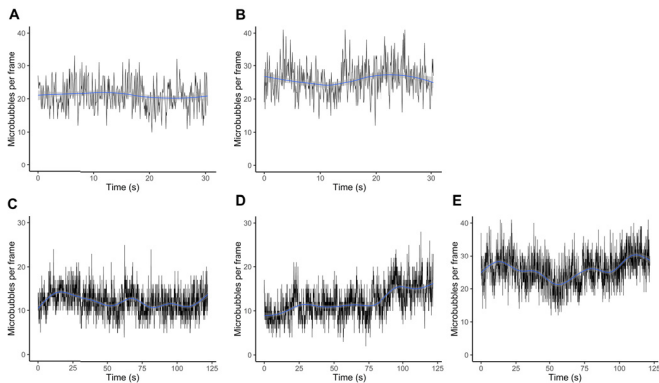


Fig. 5. Number of MBs detected per confocal frame. (a) and (b) were from a shorter pilot imaging set from the same CAM. (c) and (d) were from the second embryo, and (e) from the final embryo in this study. The average of the five imaging acquisitions yielded an average of 19.4 ± 4.2 MBs per confocal FOV.

produce saturation curves, as demonstrated in Fig. 7. We then generated empirical wash-in curves for the confocal data using a temporal maximum intensity projection of the MB centroid positions (see Fig. 8). The following monoexponential wash-in function was fit to all data sets:

$$C(t) = C_0(1 - e^{-\kappa t}) \quad (1)$$

where C_0 is the saturation level of the curve (assumed to be 100% of the vascular lumen), t is time in seconds, and κ is a rate constant. The abovementioned model was taken

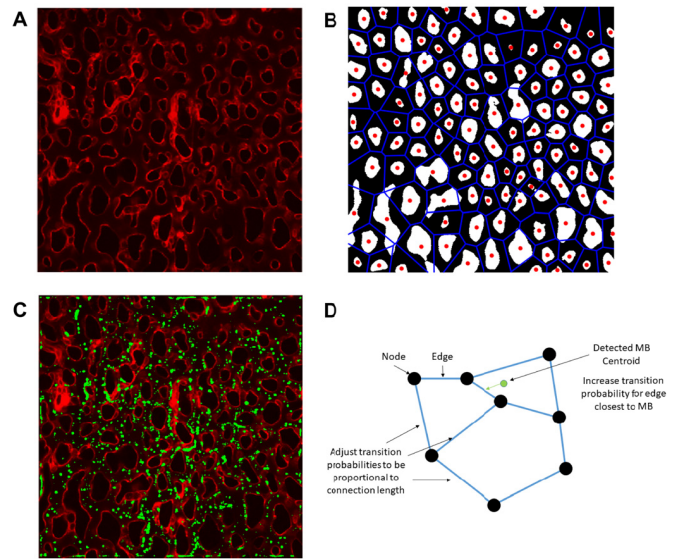


Fig. 6. (a) Isolated rhodamine channel data were used to estimate the vascular volume and number of capillary “segments” within the confocal FOV. (b) Corresponding Voronoi tessellation of the centroids (red dots) of the CAM stromal space (white segmentation). The detected paths (blue lines) were used as an estimate for the number and length of capillaries in the CAM model. (c) Temporal MB centroid projection (green) on CAM microvasculature (red). (d) Diagrammatic example of network edge weighting adjustments, where transition probabilities were altered to account for connection lengths and detect MB centroids.

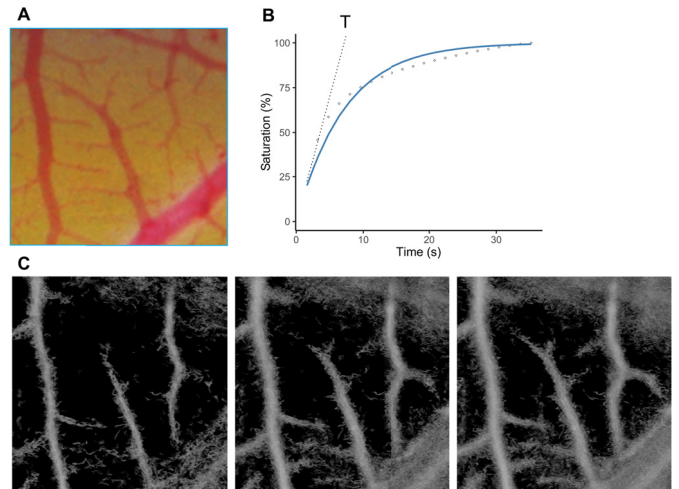


Fig. 7. (a) Reference optical image of a ULM region of interest. (b) ULM accumulation saturation curve, yielding a characteristic time of 7.1 s (21.4-s saturation time). (c) Example ULM images taken at different time steps (1.6, 6.4, and 22.4 s) to demonstrate gradual saturation of the reconstruction.

as equivalent to the exponential saturation model used by Dencks *et al.* [12].

E. Discrete-Time Markov Chain Monte Carlo Simulations

As an alternative technique to estimate the time to full perfusion, we represented the CAM vessel bed as an empirically determined undirected discrete-time Markov chain network. This permitted us to examine the effect of adjusting the network transition weights on the overall perfusion time for

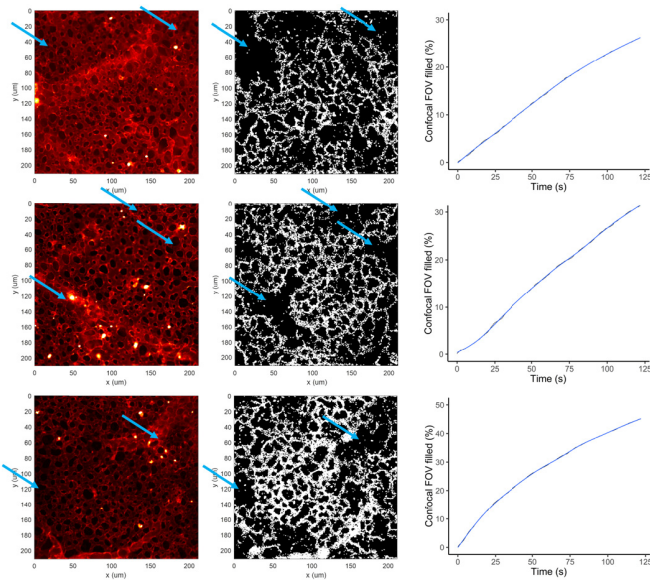


Fig. 8. CAM microvasculature (red) with temporal MB centroid projections (gray). The arrows highlight the regions with few MB passage events, indicating rarely perfused capillaries. (right column) The cumulative area of the confocal FOV filled with MBs during the acquisition, with a fit curve.

a physiologically relevant topology. The network adjacency matrix was constructed via Voronoi tessellation (“voronoi.m” in MATLAB) of CAM stromal space centroids (see Fig. 6), where network nodes were defined as the endpoint intersections of Voronoi line segments. Monte Carlo random walks on this empirically determined network were initialized by randomly selecting a starting node position from a uniform distribution for the “walker’s” location, representing a single MB in the capillary bed. Each subsequent step of the MB walker was performed by randomly selecting a neighboring network node with the transition probability weighted by the network adjacency matrix. This was done to estimate the cover time of the network nodes (vertices) and the network edges (connections), where edge cover time is indicative of MB traversal in all capillary segments and thus the 90% saturation time.

It is worth noting that a discrete-time Markov chain network with unweighted transition probabilities represents the lower bound for cover times. In order to get a more realistic estimate for the time to traverse the Markov chain network, we adjusted the relative weighting, or traversal probabilities, for each network edge. Briefly, for each node position, we adjusted the normalized edge transition probabilities to be proportionate to the relative connection lengths, such that longer vessels had proportionally lower transition probabilities. This was referred to as the distance-weighted network. We also produced network weightings where the edge transition probabilities were proportional to the number, or density, of detected MB centroids from the confocal images. This centroid-weighted network had a substantial bias to select few “high flow” vascular pathways, capturing the flow heterogeneity observed in the confocal video. A diagrammatic example of this weighting procedure is depicted in Fig. 6. Finally, we combined the

two weighted adjacency matrices together via a normalized Hadamard product to account for both features simultaneously.

III. RESULTS

A. Ultrasound Localization Microscopy

ULM imaging of the CAM vessel bed was able to accurately localize microvascular flow within arterioles and venules with diameters on the order of tens of microns, as confirmed by optical imaging (see Fig. 2). The characteristic hexagonal shape of the CAM microvasculature was partially recovered by ULM imaging; however, we failed to reconstruct all of the vascular features on the scale of capillaries ($<10\ \mu\text{m}$). When reviewing the SVD filtered IQ cineloops, we were able to observe MB signals within inflowing and outflowing vasculature, but much of the MB signal disappeared during traversal of the capillary bed (Video 1). The planar nature of the CAM is such that there must be a direct capillary connection between arterioles and venules, implying that there must be a change in the MB backscatter during the capillary passage.

B. MB Flow Kinetics

Confocal imaging demonstrated a polydisperse size distribution of FITC-labeled MBs, as shown in Figs. 3 and 4. The median diameter of MBs was found to be $2.5\ \mu\text{m}$, which is within the range reported by the manufacturer ($2.3\text{--}2.9\ \mu\text{m}$) (VisualSonics PN11691). The largest observed MB diameter was $6.7\ \mu\text{m}$, potentially indicating MB aggregation. The eGFP channel cross correlation technique outlined in Section II-C yielded an average of 19.4 ± 4.2 MBs per confocal FOV, as shown in Fig. 5. An example of MB tracking on confocal data can be seen in Video 2. In order to validate this observation, we first estimated the blood volume of the CAM membrane using the rhodamine channel data. Manual segmentation of the vascular space found that approximately 76% of the confocal FOV comprised of vascular lumen and yielded an estimate for blood volume of $3.4 \times 10^5\ \mu\text{m}^3$ or $3.4 \times 10^{-4}\ \mu\text{L}$ of blood, assuming that the membrane thickness is $10\ \mu\text{m}$. This relatively high area percentage of the vascular lumen was expected as the CAM is analogous to lung tissue for the developing embryo and, therefore, requires a high blood-to-surface area ratio for efficient gas exchange.

Given that the injection volume of MBs was $70\ \mu\text{L}$ and that the reported concentration of Vevo Micromarker is 2×10^9 MB/mL, we can assume that the total number of injected MBs is on the order of 1.4×10^8 MBs per bolus. Chicken embryos at this stage of development (EDD-18) have an approximate total blood volume of $2.5\ \text{mL}$ [17]. Thus, we estimate that the MB concentration in chicken blood was 5.6×10^7 MBs per mL of blood. Multiplying this result with the estimate of blood volume in the confocal FOV yields an estimate of 19.1 MBs per confocal imaging frame. This result, in combination with the finding that some of the detected MBs diameters were less than $1\ \mu\text{m}$ could be taken as evidence that some MB rupture may have occurred following the bolus injection into CAM vasculature (i.e., the smallest detected MBs may be phospholipid shell fragments). One can also

note the bimodal nature of the MB size distribution, with a subpopulation of large diameter MBs. We speculate that these represent MB aggregates (see Fig. 3).

C. Estimated Time to Fully Perfuse Capillary Bed

The fitting for the confocal data yielded an average rate constant $\kappa = 2.21 \times 10^{-4} \text{ s}^{-1}$, which corresponds to an estimated 708 s required to reach a 90% vascular perfusion. Applying this rate constant directly overestimates the time for total perfusion, as our confocal imaging acquisition was temporally sparse (14.7 Hz) relative to the typical flow speeds found in capillaries ($\sim 1 \text{ mm/s}$). The ideal minimum frame rate would be one in which no new pixels occupied by moving MBs are missed during the idle time between two consecutive confocal frames. We posit that this frame rate would correspond to an MB moving by half its diameter per time step, and thus, by temporally interpolating our maximum intensity projection by this factor, we will be able to recover the missing MB signals that would have been captured with such frame rate. Using the median of MB diameters found in this study ($2.5 \mu\text{m}$) and an assumed MB velocity of 1 mm/s , this corresponds to a minimum time step of 1.25 ms or a frame rate of 800 Hz. This then yields an estimated time to 90% perfusion of 13 s based on the rate constant derived from (1).

Hingot *et al.* [6] found a characteristic time of 76.8 s for ULM reconstructions at a pixel size of $5 \mu\text{m}$, corresponding to a saturation time of 230.4 s (defined as 90% perfusion). However, their experiment involved the injection of $400 \mu\text{L}$ of Sonovue (average concentration of $3 \times 10^8 \text{ MBs/mL}$ [18]) into a 500-g rat. The circulating blood volume in rats is estimated to be 64 mL/kg [19], leading to an MB concentration of $3.75 \times 10^6 \text{ MBs per mL}$ of blood in their experiment. This is roughly 14.9 times lower than our MB concentration of $5.6 \times 10^7 \text{ MBs per mL}$ of blood, as detailed earlier. Linearly scaling our estimates by this difference in MB concentration yields time to 90% perfusion of 193 s and corresponding characteristic time of 64.3 s. Likewise, the report by Dencks *et al.* [12] used a $50\text{-}\mu\text{L}$ bolus of MBs at a concentration of $2 \times 10^8 \text{ MBs/mL}$. The estimated blood volume for a 25 g mouse is around 1.8 mL [19], yielding an MB blood concentration of $5.56 \times 10^6 \text{ MBs/mL}$ of blood. Scaling our estimates by this ratio of MB concentration results in a 90% perfusion time of 131 s.

The saturation curves generated from the ULM data set (see Fig. 7) generated an average rate constant of $\kappa = 0.14 \text{ s}^{-1}$. This corresponds to a characteristic time of 7.1 s and a 90% perfusion time of 21.4 s. Scaling these results by the difference in MB concentration yields a characteristic time of 106 s, with a saturation time of 319 s. It is worth noting that the high concentration of MBs used in this study necessitated discarding several overlapping MB events, potentially extending the saturation time.

D. Monte Carlo Simulation Perfusion Times

A Voronoi tessellation of the CAM vessel bed, as shown in Fig. 6, yielded a total of 225 vertices (branching points) and 345 connections (or capillary segments) with a median length

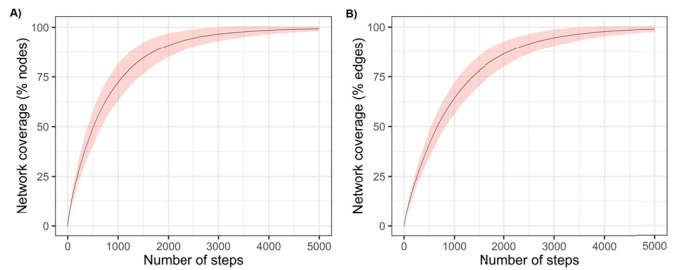


Fig. 9. Cover times for 1000 Monte Carlo simulations of a discrete-time Markov chain network generated using Voronoi tessellation of the CAM vessel bed. (a) Coverage of network nodes. (b) Coverage for the network edges. The solid line is the mean result, and the band is the standard deviation of the simulations.

of $14.1 \mu\text{m}$. The results of 1000 Monte Carlo simulations on this network are demonstrated in Fig. 9.

The average 90% edge cover time of this discrete-time Markov chain network was found to be 31.7 s (2260 walker steps), under the assumption of an MB velocity of 1 mm/s and a measured median edge length of $14.1 \mu\text{m}$. Given that the cover time for k independent walkers (i.e., MBs in the network) is linearly proportional to the cover time of a single walk [20], we can scale this result by the number of MBs detected per frame. Thus, we estimate that it would take just 1.64 s for 19.4 MBs to traverse this network. Adjusting this result to the difference in MB concentration from the article by Hingot *et al.* [6] yields a total perfusion time of 24.5 s.

As mentioned earlier, a discrete-time Markov chain network with unweighted transition probabilities will have the fastest cover times of this topology. Thus, we used the edge path lengths and detected MB centroids (see Fig. 6) to adjust the relative weighting (or traversal probabilities) for each network edge, as described in Section II-E. Adjusting the weighting of the adjacency matrices had a net effect of increasing the network coverage times (see Table I).

The average edge cover time of the distance-weighted network was 4790 steps, which corresponds to a traversal time of 51.8 s under the assumptions outlined for the unweighted Markov-chain network mentioned earlier. The 90% coverage time for the centroid-weighted network was 8150 steps, yielding a saturation time of 88.3 s. Finally, the combined weighted network had the longest coverage time at 16 800 steps. This corresponds to a saturation time of 182 s, which is on the same order of magnitude as the values reported by Hingot *et al.* [6], Christensen-Jeffries *et al.* [7], and Dencks *et al.* [12]. These results are summarized in Table I, along with their corresponding MB concentrations. Table I reports the direct estimates of MB 90% perfusion time, in addition to the 90% perfusion times adjusted to a common blood concentration (the MB concentration reported by Hingot *et al.* [6]).

IV. DISCUSSION

In this pilot study, we reported the time kinetics of fluorescently labeled MBs in capillary-level microvasculature as measured via confocal microscopy. We observed $19.4 \pm 4.2 \text{ MBs}$ per confocal field of view ($212 \mu\text{m} \times 212 \mu\text{m}$), which is in excellent agreement to the expected blood flow-rate count of

TABLE I
ESTIMATED SATURATION TIMES

Method	Microbubble Concentration (MBs per mL blood)	Time to 90% MB perfusion (seconds)	MB perfusion time adjusted to common blood concentration (seconds)
Dencks <i>et al.</i> [12]	5.56×10^6	101	150
Christensen-Jeffries <i>et al.</i> [7]	5.56×10^6	139	206
Hingot <i>et al.</i> [6]	3.75×10^6	230.4	230.4
ULM CAM saturation	5.6×10^7	21.4	319
Confocal wash-in	5.6×10^7	13	193
Markov-chain (unweighted)	5.6×10^7	1.6	24.5
Markov-chain (distance-weighted)	5.6×10^7	3.5	51.8
Markov-chain (centroid-weighted)	5.6×10^7	5.9	88.3
Markov-chain (distance- and centroid-weighted)	5.6×10^7	12.2	182

19.1 MBs per frame. The estimated time for MBs to traverse this capillary network was 193 s based on wash-in curves generated from the confocal data and 182 s for a discrete-time Markov chain Monte Carlo simulation where the network transition probabilities were weighted by vessel length and MB centroid density. Saturation curves of our ULM data set yielded a time estimate of 319 s. These results are consistent with the characteristic time for 5- μ m ULM reconstruction reported by Hingot *et al.* [6] and on the same order of magnitude as the 90% exponential saturation time reported by Dencks *et al.* [12] and the generalized MB perfusion model developed by Christensen-Jeffries *et al.* [7].

While ULM imaging of the CAM was able to accurately localize microvascular flow down to the tens of microns scale (i.e., arterioles and venules), we had difficulty fully reconstructing capillary-level MB flow in the CAM (see Fig. 2). This is surprising given the high density of MBs found within the relatively small FOV of confocal imaging. Interestingly, we were able to observe MBs on B-mode images and with ULM from both inflowing and outflowing vasculature, but the MB signal became silent during traversal of the capillary bed. One possible explanation is that low capillary compliance is prohibiting the volumetric oscillations of MBs [8]–[11], resulting in reduced signal backscatter. The effect of confinement leading to a reduction in MB oscillation has been previously reported in chicken embryos [21], and this may be compounded by the relatively low hydrostatic pressure in CAM capillary vessels.

Laser-scanning confocal imaging was used as the gold standard in this study to confirm the blood-flow kinetics of MBs as they traversed the CAM capillary bed. However, the framerate achieved in our experimental design for a $212 \mu\text{m} \times 212 \mu\text{m}$ FOV was slow (14.7 Hz) relative to the expected speed of MBs ($\sim 1 \text{ mm/s}$). This low framerate is an inherent limitation of the two-wavelength resonant confocal imaging used in this study. As a consequence, the fluorescent imaging presented in this study may have missed some of the MB passage events. We attempted to correct for this by scaling our temporally sparse acquisition by a hypothetical ideal minimum frame rate to recover more realistic estimates of total perfusion times.

Although this approach produced perfusion estimates that are consistent with the literature (193 s versus 230.4 s [6]), it is not an ideal solution given that it cannot account for completely missed MB events. Furthermore, the low framerate may have influenced the weightings applied to centroid-weighted Markov-chain simulation, as MB passage through particularly fast vessels may have been missed. Confocal imaging is also limited in its ability to accurately measure MB diameters as the narrow imaging slab thickness might intersect MB at various heights. This, in turn, may explain the wide distribution of MB diameters seen in Fig. 4.

Another limitation of this study is the high concentration of MBs used in both ULM and optical imaging. This invariably leads to a substantial amount of MB signal overlap for ULM reconstruction, increasing the localization uncertainty and necessitating a longer acquisition time. This may, in part, explain the relatively high estimate for ULM 90% saturation time found in this study (319 s). Furthermore, the assumption that all saturation times can be linearly scaled by the difference in MB concentration requires that passage of individual MBs are independent of one another and is potentially an oversimplification of more complicated MB flow kinetics and interactions (e.g., aggregation). Finally, it can be speculated that the saturation rate may be dependent on tissue physiology and/or the local metabolic rate. As such, it would be expected that there would be differences in the 90% saturation time for tumors, brain tissue, and the CAM membrane.

As an alternate technique to estimate perfusion times, we modeled the CAM capillary bed as a discrete-time Markov-chain. Different network weightings were proposed based on quantified data derived from the confocal images, such as vessel segment length and number of nearby MB centroids. We found that the edge coverage times for these networks was shorter than either confocal or ultrasound-based estimates of perfusion time. In general, we would anticipate that a Markov-chain Monte Carlo simulation would underestimate the perfusion time for a capillary network given that MBs are assumed to be moving in a constant velocity from node-to-node and that the simulation assumes that all MBs passing through a capillary will be successfully detected, localized,

and tracked. In comparison, for ULM imaging, a large number of MB events are typically discarded to avoid false-positive detections and overlapping MB signals. These localization uncertainties would necessarily increase the acquisition times required to fully reconstruct a super-resolution image of a capillary bed.

V. CONCLUSION

Confocal imaging of fluorescently labeled MBs in capillary vessels is consistent with a probability-derived explanation for the long acquisition times required for ultrasound localization imaging. Our study suggests that it may be challenging to accurately depict the capillary bed with ULM given the large quantity of MBs that coexist in a minute FOV and the localization uncertainties associated with high MB concentration. Furthermore, low capillary compliance and low hydrostatic pressure may further exasperate efforts to reconstruct capillary-level flow by interfering with MB volumetric oscillations.

ACKNOWLEDGMENT

The authors would like to thank Prof. Mark Borden from the University of Colorado for his insightful discussion on MB backscatter characteristics in the microvasculature. The content is solely the responsibility of the authors and does not necessarily represent the official views of the NIH.

REFERENCES

- [1] C. Errico *et al.*, "Ultrafast ultrasound localization microscopy for deep super-resolution vascular imaging," *Nature*, vol. 527, no. 7579, pp. 499–502, Nov. 2015, doi: [10.1038/nature16066](https://doi.org/10.1038/nature16066).
- [2] O. Couture, V. Hingot, B. Heiles, P. Muleki-Seya, and M. Tanter, "Ultrasound localization microscopy and super-resolution: A state of the art," *IEEE Trans. Ultrason., Ferroelectr., Freq. Control*, vol. 65, no. 8, pp. 1304–1320, Aug. 2018, doi: [10.1109/TUFFC.2018.2850811](https://doi.org/10.1109/TUFFC.2018.2850811).
- [3] T. Opacic *et al.*, "Motion model ultrasound localization microscopy for preclinical and clinical multiparametric tumor characterization," *Nature Commun.*, vol. 9, no. 1, p. 1527, Dec. 2018, doi: [10.1038/s41467-018-03973-8](https://doi.org/10.1038/s41467-018-03973-8).
- [4] K. Christensen-Jeffries, R. J. Browning, M.-X. Tang, C. Dunsby, and R. J. Eckersley, "*in vivo* acoustic super-resolution and super-resolved velocity mapping using microbubbles," *IEEE Trans. Med. Imag.*, vol. 34, no. 2, pp. 433–440, Feb. 2015, doi: [10.1109/TMI.2014.2359650](https://doi.org/10.1109/TMI.2014.2359650).
- [5] P. Song *et al.*, "Improved super-resolution ultrasound microvessel imaging with spatiotemporal nonlocal means filtering and bipartite graph-based microbubble tracking," *IEEE Trans. Ultrason., Ferroelectr., Freq. Control*, vol. 65, no. 2, pp. 149–167, Feb. 2018, doi: [10.1109/TUFFC.2017.2778941](https://doi.org/10.1109/TUFFC.2017.2778941).
- [6] V. Hingot, C. Errico, B. Heiles, L. Rahal, M. Tanter, and O. Couture, "Microvascular flow dictates the compromise between spatial resolution and acquisition time in ultrasound localization microscopy," *Sci. Rep.*, vol. 9, no. 1, p. 2456, Dec. 2019, doi: [10.1038/s41598-018-38349-x](https://doi.org/10.1038/s41598-018-38349-x).
- [7] K. Christensen-Jeffries *et al.*, "Poisson statistical model of ultrasound super-resolution imaging acquisition time," *IEEE Trans. Ultrason., Ferroelectr., Freq. Control*, vol. 66, no. 7, pp. 1246–1254, Jul. 2019, doi: [10.1109/TUFFC.2019.2916603](https://doi.org/10.1109/TUFFC.2019.2916603).
- [8] C. F. Caskey, S. M. Stieger, S. Qin, P. A. Dayton, and K. W. Ferrara, "Direct observations of ultrasound microbubble contrast agent interaction with the microvessel wall," *J. Acoust. Soc. Amer.*, vol. 122, no. 2, pp. 1191–1200, Aug. 2007, doi: [10.1121/1.2747204](https://doi.org/10.1121/1.2747204).
- [9] K. Kooiman, H. J. Vos, M. Versluis, and N. de Jong, "Acoustic behavior of microbubbles and implications for drug delivery," *Adv. Drug Del. Rev.*, vol. 72, pp. 28–48, Jun. 2014, doi: [10.1016/j.addr.2014.03.003](https://doi.org/10.1016/j.addr.2014.03.003).
- [10] D. H. Thomas, V. Sboros, M. Emmer, H. Vos, and N. De Jong, "Microbubble oscillations in capillary tubes," *IEEE Trans. Ultrason., Ferroelectr., Freq. Control*, vol. 60, no. 1, pp. 105–114, Jan. 2013, doi: [10.1109/TUFFC.2013.2542](https://doi.org/10.1109/TUFFC.2013.2542).
- [11] T. G. Leighton, "The inertial terms in equations of motion for bubbles in tubular vessels or between plates," *J. Acoust. Soc. Amer.*, vol. 130, no. 5, pp. 3333–3338, Nov. 2011, doi: [10.1121/1.3638132](https://doi.org/10.1121/1.3638132).
- [12] S. Dencks, M. Piepenbrock, G. Schmitz, T. Opacic, and F. Kiessling, "Determination of adequate measurement times for super-resolution characterization of tumor vascularization," in *Proc. IEEE Int. Ultrason. Symp. (IUS)*, Sep. 2017, pp. 1–4, doi: [10.1109/ULTSYM.2017.8092351](https://doi.org/10.1109/ULTSYM.2017.8092351).
- [13] S. M. Jilani, T. J. Murphy, S. N. M. Thai, A. Eichmann, J. A. Alva, and M. L. Iruela-Arispe, "Selective binding of lectins to embryonic chicken vasculature," *J. Histochem. Cytochem.*, vol. 51, no. 5, pp. 597–604, May 2003, doi: [10.1177/002215540305100505](https://doi.org/10.1177/002215540305100505).
- [14] Y. Desailly, J. Pierre, O. Couture, and M. Tanter, "Resolution limits of ultrafast ultrasound localization microscopy," *Phys. Med. Biol.*, vol. 60, no. 22, pp. 8723–8740, Nov. 2015, doi: [10.1088/0031-9155/60/22/8723](https://doi.org/10.1088/0031-9155/60/22/8723).
- [15] Y. Desailly, A.-M. Tissier, J.-M. Correas, F. Wintzenrieth, M. Tanter, and O. Couture, "Contrast enhanced ultrasound by real-time spatiotemporal filtering of ultrafast images," *Phys. Med. Biol.*, vol. 62, no. 1, pp. 31–42, Jan. 2017, doi: [10.1088/1361-6560/62/1/31](https://doi.org/10.1088/1361-6560/62/1/31).
- [16] B. Zhang, J. Zerubia, and J.-C. Olivo-Marin, "Gaussian approximations of fluorescence microscope point-spread function models," *Appl. Opt.*, vol. 46, no. 10, p. 1819, Apr. 2007, doi: [10.1364/ao.46.001819](https://doi.org/10.1364/ao.46.001819).
- [17] C. Kind, "The development of the circulating blood volume of the chick embryo," *Anatomy Embryology*, vol. 147, no. 2, pp. 127–132, Aug. 1975.
- [18] M. Schneider, "Characteristics of SonoVue trade mark," *Echocardiography*, vol. 16, no. 7, pp. 743–746, Oct. 1999.
- [19] K.-H. Diehl *et al.*, "A good practice guide to the administration of substances and removal of blood, including routes and volumes," *J. Appl. Toxicol.*, vol. 21, no. 1, pp. 15–23, Jan. 2001.
- [20] C. Cooper, A. Frieze, and T. Radzik, "Multiple Random Walks in Random Regular Graphs," *SIAM J. Discrete Math.*, vol. 23, no. 4, pp. 1738–1761, Jan. 2010, doi: [10.1137/080729542](https://doi.org/10.1137/080729542).
- [21] T. Faez, I. Skachkov, M. Versluis, K. Kooiman, and N. de Jong, "*In vivo* characterization of ultrasound contrast agents: Microbubble spectroscopy in a chicken embryo," *Ultrasound Med. Biol.*, vol. 38, no. 9, pp. 1608–1617, Sep. 2012, doi: [10.1016/j.ultrasmedbio.2012.05.014](https://doi.org/10.1016/j.ultrasmedbio.2012.05.014).



Matthew R. Lowerison received the Ph.D. degree in medical biophysics from the University of Western Ontario, London, ON, Canada, in 2017.

He is currently with the Department of Electrical and Computer Engineering, Beckman Institute for Advanced Science and Technology, University of Illinois at Urbana–Champaign, Urbana, IL, USA. His current research interests include ultrasound microvessel imaging, super-resolution ultrasound localization microscopy (ULM), and

the ultrasonic characterization of tumor microenvironments.



Chengwu Huang (Member, IEEE) received the B.S. degree in biomedical engineering from Beihang University, Beijing, China, in 2012, and the Ph.D. degree from the Department of Biomedical Engineering, Tsinghua University, Beijing, in 2017.

He is currently with the Department of Radiology, Mayo Clinic College of Medicine, Rochester, MN, USA. His current research interests include ultrasound microvessel imaging and ultrasound elastography.



Yohan Kim received the Ph.D. degree in pathology and laboratory medicine from the University of Western Ontario, London, ON, Canada, in 2020.

He is currently with the Department of Urology, Mayo Clinic, Rochester, MN, USA. His current research interests include high-resolution confocal imaging of microvessel, cancer extracellular vesicle, and nanoscale flowcytometry-based liquid biopsy of cancer extracellular vesicles.



Shigao Chen (Senior Member, IEEE) received the B.S. and M.S. degrees in biomedical engineering from Tsinghua University, Beijing, China, in 1995 and 1997, respectively, and the Ph.D. degree in biomedical imaging from Mayo Graduate School, Rochester, MN, USA, in 2002.

He is currently a Professor with the Mayo Clinic College of Medicine. His research interest is noninvasive quantification of the viscoelastic properties of soft tissue using ultrasound, and ultrasound microvessel imaging.



Fabrice Lucien received the B.S. degree in biological sciences and the Ph.D. degree in immunology from the University of Sherbrooke, Sherbrooke, QC, Canada, in 2007 and 2017, respectively.

He is currently an Assistant Professor with the Department of Urology, Mayo Clinic College of Medicine, Rochester, MN, USA. His current research interests are the characterization of the tumor metabolic and immune microenvironment, development of cancer liquid biopsies, and high-resolution/nanoscale flow cytometry.



Pengfei Song (Senior Member, IEEE) received the B.Eng. degree in biomedical engineering from the Huazhong University of Science and Technology, Wuhan, China, in 2008, the M.S. degree in biological systems engineering from the University of Nebraska-Lincoln, Lincoln, NE, USA, in 2010, and the Ph.D. degree in biomedical sciences-biomedical engineering from the Mayo Graduate School, Mayo Clinic College of Medicine, Rochester, MN, USA, in 2014.

He is currently an Assistant Professor with the Department of Electrical and Computer Engineering, Beckman Institute for Advanced Science and Technology, University of Illinois at Urbana-Champaign, Urbana, IL, USA. His current research interests are super-resolution ultrasound microvessel imaging, ultrafast 3-D imaging, deep learning, functional ultrasound, and ultrasound shear wave elastography.

Dr. Song is a full member of the Acoustical Society of America (ASA) and a member of the American Institute of Ultrasound in Medicine (AIUM) and Sigma Xi.